Atmospheric Environment 202 (2019) 345–356

Contents lists available at ScienceDirect

Atmospheric Environment

journal homepage: www.elsevier.com/locate/atmosenv

Long-term aerosol size distributions and the potential role of volatile organic compounds (VOCs) in new particle formation events in Shanghai

Yan Ling[a], Yanyu Wang[a], Junyan Duan[a], Xin Xie[a], Yuehui Liu[a], Yarong Peng[a], Liping Qiao[b,**], Tiantao Cheng[c,a,d,*], Shengrong Lou[b], Hongli Wang[b], Xiang Li[a], Xuhuang Xing[e]

[a] Shanghai Key Laboratory of Atmospheric Particle Pollution and Prevention (LAP^3), Department of Environmental Science and Engineering, Institute of Atmospheric Sciences, Fudan University, Shanghai, 200438, China
[b] State Environmental Protection Key Laboratory of Formation and Prevention of Urban Air Pollution Complex, Shanghai Academy of Environmental Sciences, Shanghai 200233, China
[c] Department of Atmospheric and Oceanic Sciences, Institute of Atmospheric Sciences, Fudan University, Shanghai, 200438, China
[d] Shanghai Institute of Eco-Chongming (SIEC), Shanghai, 200062, China
[e] Hainan Meteorological Bureau, Haikou, 570203, China

ARTICLE INFO

Keywords:
Aerosol
Size distribution
New particle formation
Volatile organic compounds

ABSTRACT

New particle formation (NPF) events are important phenomena that generate nanoparticles and even fine particles via gas-to-particle conversion. These events have clear effects on aerosol loading, atmospheric chemistry and global climate. Long-term field measurements were used to characterize aerosol size distributions and to examine the role of atmospheric volatile organic compounds (VOCs) in NPF events in the urban environment of Shanghai. Aitken and accumulation particles are dominant and account for 85–95% of the total particles, whereas coarse particles are negligible. Particles in the four size-models show the same seasonality: highest in winter and lowest in autumn. The mean particle size distributions display different patterns of diurnal fluctuation, including bimodal in spring and winter, tri-modal in autumn, and "banana" shaped in summer due to highly frequent NPF events. The geometric mean diameter (GMD) is often 20–30 nm or 40–60 nm. Overall, NPF events occur on 89 days out of 335 measurement days (26.5%), and the newly formed particles have a mean growth rate of 6.28 nm h^{-1}. Two typical anthropogenic aromatics, benzene and toluene, from traffic emissions closely match the occurrence of NPF events and have a weakly positive correlation with the nucleation particle number concentrations. The enhanced VOCs as precursors of organic vapors may contribute to the growth process of NPF events to some extent (e.g., growth rate) so that newly formed particles can grow into a detectable size.

1. Introduction

Aerosols can directly affect climate through scattering and absorbing solar and ground radiation as well as indirectly affect climate through acting as cloud condensation nuclei (CCN) or ice nuclei (IN) that participate in precipitation processes and in cloud. Anthropogenic aerosols are known as the biggest uncertainties in estimating global climate change (Penner et al., 2004; Seinfeld and Pandis, 2006). Furthermore, aerosol particles can cause adverse health effects through changes in human pulmonary function and respiratory irritation in the surface atmosphere, especially during heavy pollution events (Sarnat et al., 2001; Penttinen et al., 2001).

A new particle formation (NPF) event is important evidence of secondary aerosol formation by gas-particle transfer in the atmosphere (Kulmala et al., 2004a,b). NPF, also known as aerosol nucleation, is considered the largest contributor of submicron particles to global aerosol loading (Spracklen et al., 2006; Pierce and Adams, 2009; Seinfeld and Pandis, 2006). To date, a number of studies have researched the nucleation and growth of NPFs by aerosol size distribution (e.g., clusters and nanometer particles) around the world, such as at pristine (Kivekäs et al., 2009; Dal Maso et al., 2007), rural (Weber et al., 1999; Creamean et al., 2011; Pikridas et al., 2012; Vakkari et al., 2011), polluted (Harrison et al., 1999; Woo et al., 2001; Hussein et al., 2004; Stanier et al., 2004a), forest (Allan et al., 2006; Han et al., 2013; Pierce

* Corresponding author. Shanghai Key Laboratory of Atmospheric Particle Pollution and Prevention (LAP^3), Department of Environmental Science and Engineering, Institute of Atmospheric Sciences, Fudan University, Shanghai, 200438, China.
** Corresponding author.
E-mail addresses: qiaolp@saes.sh.cn (L. Qiao), 16210740008@fudan.edu.cn (T. Cheng).

https://doi.org/10.1016/j.atmosenv.2019.01.018
Received 14 September 2018; Received in revised form 7 January 2019; Accepted 8 January 2019
Available online 28 January 2019
1352-2310/

et al., 2012) and polar sites (Koponen et al., 2003; Asmi et al., 2010). In general, NPF requires essential coagulation and a sink for condensable vapors, and its occurrence frequency varies with location and time. However, in urban environments, in spite of rich gaseous precursors, NPF events are rare because there are more pre-existing particles that impede nucleation and new particle growth (Wu et al., 2008; Du et al., 2012; Siingh et al., 2013). For polluted cities in economically developing regions, in particular, there is a substantial challenge to fully understand the complex mechanisms of NPFs (Yue et al., 2013; Wang et al., 2014).

Atmospheric volatile organic compounds (VOCs) generally play an essential role in NPF. Growing evidence shows that the condensation and coagulation of low volatility organic compounds are vital for NPFs (Metzger and Finlayson-Pitts, 2010). In fact, the formation of new particles is, to some extent, initiated by intense solar radiation, atmospheric gas photo-oxidation, and nucleation precursors, as well as especially high concentrations of low-volatile vapors (Wang et al., 2015). For instance, sulfuric acid, ammonia and amines have been found to play dominant roles in atmospheric nucleation, as well as the potentially heterogeneous reactions of organics on particle surfaces (Kulmala et al., 2006; Xiao et al., 2015). NPF events have been found to occur efficiently over European countries, eastern Asia as well as some parts of northern America due to the concurrent anthropogenic VOCs and SO_2 emissions in these areas. Some studies have shown that NPF events are enhanced in the anthropogenic plumes by high concentrations of SO_2 and CO that indicate the presence of VOCs (Zhang et al., 2004b). Field measurements and laboratory studies have provided extensive new insight showing that BVOCs (biogenic volatile organic compound) and AVOCs (Anthropogenic volatile organic compound) participate in nucleation and potentially contribute to NPFs (Kulmala et al., 2004a; Hatch et al., 2011; Guo et al., 2012). A clear positive correlation between the growth rate (GR) of nucleation particles and monoterpene under specific conditions has been observed in boreal forests, where large amounts of BVOCs are emitted from vegetation (Tatekawa et al., 2011). Monoterpene may have a weak effect on NPF compared to light intensity in polluted urban environments (Wang et al., 2015). The role of VOCs in NPF is still an open discussion.

In this study, measurements of size-resolved aerosol number concentrations over the course of 1 year are presented to characterize the aerosol size distribution on daily and monthly time scales in Shanghai. The aim is to focus on apparent NPFs and to give some insight into the role of VOCs in these events in urban environments.

2. Data and methodology

2.1. Observation location and instruments

All measurements were conducted at an urban site located on the campus of the Shanghai Academy of Environmental Sciences (31.18°N, 121.43°E) during 2013. The observation station, located on the 9th floor of a building, is close to residential areas but not to arterial traffic and is normally only affected by the residential emissions.

The size-resolved number concentrations of particles within the scope of 13.6–6335 nm were measured by an integrated system of a SMPS (Scanning Mobility Particle Sizer, TSI Model 3772) and an APS (Aerodynamic Particle Sizer, TSI Model 3321). Before entering the inlet, ambient air was dried using a silica gel dryer. The SMPS, consisting of a DMA (differential mobility analyzer) and a CPC (condensation particle counter), measured particle sizes between 13.6 nm and 736.5 nm. The SMPS and APS data are recorded by AIM (Aerosol Instrument Management) software from the TSI company. The SMPS (TSI corp.) is employed to track the size distribution change, in which the CPC (TSI corp.) is used to count the number of particle of each size bin. The neutralizer (TSI corp.) is used in the system to provide known charge on the particles going into the SMPS. Both multiple charge and the diffusion correction is applied when we obtained the data. The APS measured the particles of 542–5425 nm, and their particle aerodynamic diameters were converted to Stokes diameters using a size correction factor α assuming the particle density of 1.36 g cm^{-3} which has been calculated for Shanghai by Yin et al. (2015). Under the spherical assumption, α is defined as $\alpha = \sqrt{\frac{\rho_P}{\chi\rho_0}}$, where ρ_P is the density of particles, ρ_0 is the reference density and χ is the shape factor. Here a shape factor (χ) of 1 was used to convert the aerodynamic diameter into a Stokes diameter according to the theory proposed by Seinfeld and Pandis (2006). Moreover, we assumed $\rho_0 = 1$ g cm^{-3} according to Khlystov et al. (2004). The loss caused by transmission efficiency was already considered and corrected for in the total particle number concentration.

A gas chromatograph system (TH-300 GC/MS) was applied to monitor 54 species of VOCs at an hourly time resolution, including types of alkanes, alkenes, alkynes and aromatics. Meteorological factors were measured at the same site. Besides, hourly concentrations of NO, NO_2, NO_X, SO_2, CO and O_3 gases and particulate matter ($PM_{2.5}$ and PM_{10}, respectively) were monitored at the Shanghai Air Quality Monitoring Country Control Point (Shanghai Normal University), which is 1.5 km from the Shanghai Academy of Environmental Sciences campus. The sites are both located in the center of Shanghai, which, to some extent, represents the urban pollution situation in Shanghai.

2.2. Calculation of variables to characterize NPFs

The condensation sink (CS) as well as the coagulation sink (CoagS) of particles are important parameters related to atmospheric NPFs (Kulmala et al., 2004b). We classified NPF events of each day into Class I, Class II and undefined using the event classification routine of Dal Maso et al. (2005) and details will be given in section 3.3. To be considered a NPF event, a distinct mode of particles with diameters smaller than 20 nm must appear and this classification is done visually and subjectively as in Dal Maso et al. (2005). In our study, we implicitly assumed that all particles range in size from 13.6 nm to 20 nm, which were viewed as nucleation mode particles, originate from secondary formation during classes I and II and from undefined NPF events other than primary emissions. The condensation rate of vapors can reflect the rate at which the condensable vapor molecules condense on preexisting aerosols (Dal Maso et al., 2002). The CS value can be calculated using formula (1),

$$CS = 2\pi D \sum_i \beta_m(d_{p,i}) d_{p,i} N_i \quad (1)$$

where D represents the diffusion coefficient of the condensing vapor, β_m is defined as the mass flux transition correction factor, here d_i and N_i are respectively the diameter and number concentration of particles in the particle size bin, as used in previous researches (Dal Maso et al., 2007; Lehtinen et al., 2007; Kulmala et al., 2012). In theory, all particle sizes should be included in the CS calculation; although some particles (< 13.6 nm or > 6326 nm) are beyond the scope of instrument detection, their impact on the CS calculation can be ignored due to their small quantities.

Since sulfuric acid is the primary condensable vapor in the urban atmosphere, the diffusion coefficient of sulfuric acid was calculated by using formula (2) (Stanier et al., 2004b; Zhang et al., 2004b; Jeong, 2009),

$$D = 5.0032 \times 10^{-6} + 1.04 \times 10^{-8} T + 1.64 \times 10^{-11} T^2 - 1.566 \times 10^{-14} T^3 \quad (2)$$

here D is the diffusion coefficient (m^2 s^{-1}), and T is the Kelvin temperature. And in this study we used T = 293.5 K in spring and autumn, T = 303.5 K in summer and T = 273.5 K in winter, which are close to the average daytime temperatures in Shanghai during the four seasons. The transition correction factor is calculated using formula (3),

$$\beta = \frac{1 + K_n}{1 + 1.677K_n + 1.333K_n^2} \quad (3)$$

$$K_n = \frac{2\lambda}{d_p} \tag{4}$$

where β_m is the function of the Knudsen number (*Kn*) that describes the character of vapor suspended on particles according to Fuchs-Sutugin expression, λ is the effective mean free path of the vapor molecules, d_p is the diameter of particles, while α is the mass accommodation factor used to describe the possibility that the vapor molecule will stick to the particle surface during the interaction between gas phase and particle phase (Seinfeld and Pandis, 2006). Here, α = 1 and λ = 108 nm was used in our study, as used in studies of Massman (1998) and Kulmala et al. (2012).

The CoagS describes the rate of particle loss by coagulation with other particles. To simplify the calculation, Lehtinen et al. (2007) suggested a relation to link CS and CoagS. The value of CS is generally calculated for each size, and it can also be useful to acquire CoagS for different size bins. The relation can be approximated using formula (5),

$$\mathrm{Coag}S_{d_p} = CS \cdot \left(\frac{d_p}{0.71}\right)^m \tag{5}$$

where the index m ranges from −1.75 to −1.5 with an average value of −1.7, while the hydrated sulfuric molecule has a diameter of 0.71. In this study we used m = −1.6, as used by Kulmala et al. (2012).

Based on the time evolution of the nucleation particle average diameter, the growth rate of newly formed particles (GR) can be calculated by formula (6) (Kulmala et al., 2004a,b),

$$GR = \frac{\Delta D_m}{\Delta t} \tag{6}$$

here D_m is mean diameter of the nucleating particles during the growth period. We calculated GR using a log-normal Gaussian fit of the nucleation particle size distribution (Kulmala et al., 2012).

The particle formation rate (FR) represents the number of particles formed per cm^3 per second of a particular size (Kulmala et al., 2007). Compared with particle formation, when the influence of coagulation and transport are small, the FR can be calculated by formula (7),

$$J_D \approx \left.\frac{\Delta N_{D,D\max}}{\Delta t}\right|_{observed} \tag{7}$$

Among them, $N_{D,Dmax}$ means the total number concentration of particles within a size range [D, D_{max}], while D_{max} is the maximum size that clusters can grow into through growth process during Δt (Kulmala et al., 2004b).

3. Results and discussion

3.1. Temporal variation of aerosol number concentrations

The observed particles were classified into four groups according to size, that is, nucleation mode ($D_m \leq 20$ nm), Aitken mode (D_m = 20–100 nm), accumulation mode (D_m = 100–2000 nm) and coarse mode ($D_m > 2$ μm) particles. To understand the characteristics of the size-resolved particles, the particle number concentrations of separated and integrated modes were calculated for the entire study period. Fig. 1 illustrates the seasonally averaged fractions of the four modes of particles. The Aitken mode particles were dominant and accounted for 60–70% of the total particles, which has been previously discovered by other studies (Woo et al., 2001; Peng et al., 2017). The second most abundant group was the accumulation mode, with mean fractions of 25–30% during the four seasons. Although coarse mode particles were taken into consideration, their fractions were too small to have a clear presence compared with those of the other groups. In general, the particles in the four modes showed the same seasonality, with the highest values observed in January or December and the lowest in February or October (Fig. 2). In particular, the nucleation and accumulation modes increased from February to May and decreased

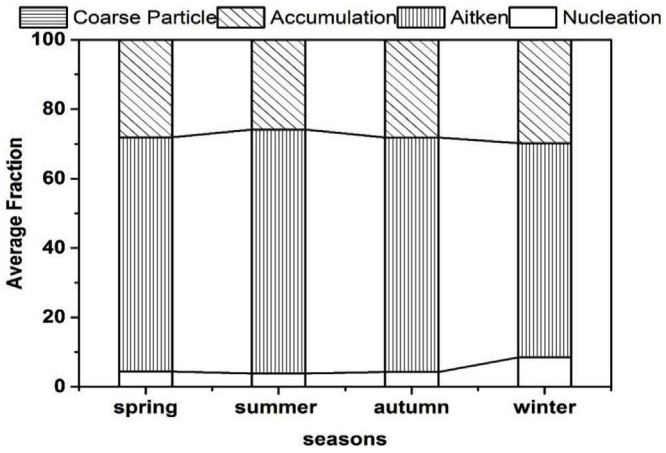

Fig. 1. Average fractions of size-model particle loadings in four seasons.

slightly until October; then, they increased again and reached a maximum. The Aitken and coarse modes experienced a similar pattern of fluctuation to the first two modes, although their maximum occurred in January rather than December.

Fig. 3 presents diurnal variations in the mean size-model particle number concentrations during the four seasons. Overall, the nucleation mode particles had one clear peak started at noon at around 13:00 LT in spring, and in winter there two morning peaks and one afternoon peaks at 8:00 LT, 13:00 LT and 18:00 LT respectively. Because of vigorous secondary formation (e.g., NPF), despite deviations in time and intensity, the morning peak of the nucleation particles appeared at 9:00–12:00 LT in summer and autumn, whereas it was delayed to 12:00–15:00 LT in spring and winter. Aitken mode particles had three peaks at approximately 8:30 LT, 13:00 LT, and 18:00 LT in spring, autumn and winter, respectively. In summer, the peak concentration of the Aitken mode particles occurred at approximately 12:00 LT, following the morning peak of the nucleation mode, which may be attributed to new particles that transformed into Aitken mode particles during NPFs. The accumulation mode particles increased from 3:00 LT to 19:30 LT in summer and had two peaks at approximately 9:00 LT and 19:30 LT in the other three seasons, possibly due to traffic emissions that correspond to times of rush-hour traffic. Overall, the Aitken mode particles largely determined the diurnal variation of the total particles, especially in the morning peak period of summer, and the particles of accumulation mode influenced the diurnal variation of total particles to some extent, especially in the afternoon peak period of winter.

Fig. 4 shows the diurnal cycles of particle number size distributions in the four seasons. The average particle number size distribution shows a clear bimodal pattern in spring and winter as well as a tri-modal pattern in autumn, with particle median diameters of 20–30 nm or 40–60 nm. A similar phenomenon has previously been found by Peng et al. (2017) and Wu et al. (2007). The peaks in particle concentration occurred during the period 07:00–09:30 LT in the morning, 11:00–14:00 LT around midday, and 17:00–23:00 LT in the afternoon to night in the spring, autumn and winter, corresponding to respective median diameters. In addition, a plume of high-particle concentrations often occurred, probably affected by the pollution between 00:00 LT and 06:00 LT, especially in autumn and winter. The morning peaks in these three seasons were attributed to NPFs and ultrafine particle emissions (e.g., vehicle exhaust) (Pérez et al., 2010). The evening peaks were also affected by traffic emissions while the size distribution is much wider (30–90 nm), which is probably due to the condensational growth of aged particles. In winter, the low boundary layer and little rainfall caused pollutant accumulation that resulted in high particle loadings (Zhang et al., 2017), and a large amount of aged accumulation particles were transported from the north during the central heating period in northern China (Li et al., 2011). Surprisingly, in summer, the

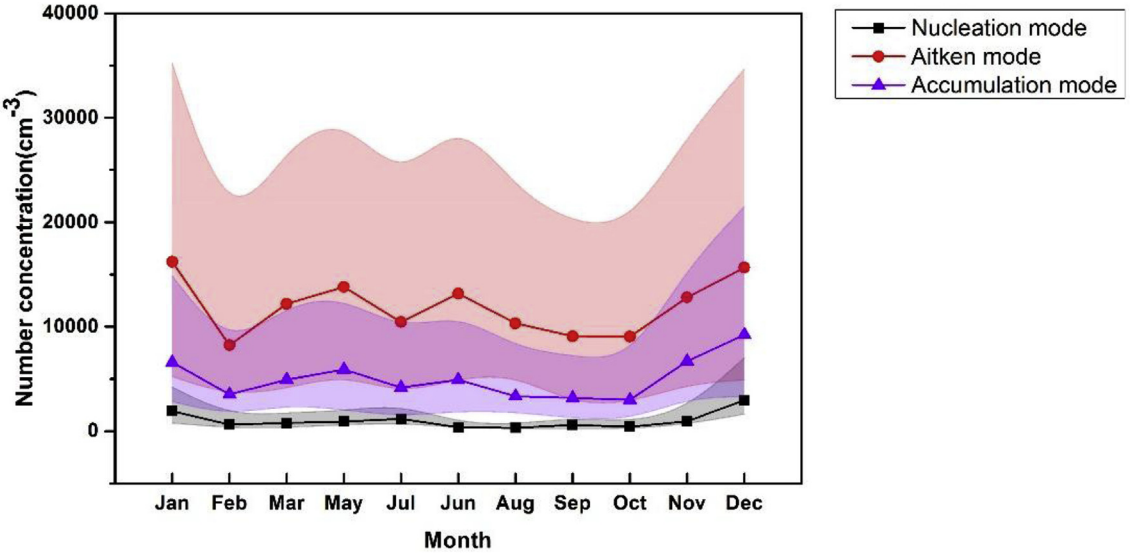

Fig. 2. Monthly size-model particle number concentrations. The solid lines are monthly mean number concentrations and the shaded areas represent 25-75th percentile range.

diurnal cycle of particle size distribution can be described as a typical "banana" shape, and the median diameter increased from 20-40 nm to 60–80 nm from approximately 10:00 LT in the morning until midday. We attributed this phenomenon to the high frequency of NPF events via chemical and photochemical reactions. High temperatures and strong solar radiation facilitate photochemical reactions, and the sulfate product will strengthen NPFs (Gao et al., 2009). These phenomena demonstrate that the newly formed particles play an essential role in the abundance of particles (Zhang et al., 2009).

3.2. Aerosol size distributions under pollution conditions

The pollution caused by pollutant emissions and atmospheric conditions provides an important chance to understand how these conditions influence the physical and chemical properties of aerosols. According to the World Meteorological Organization (WMO), visibility

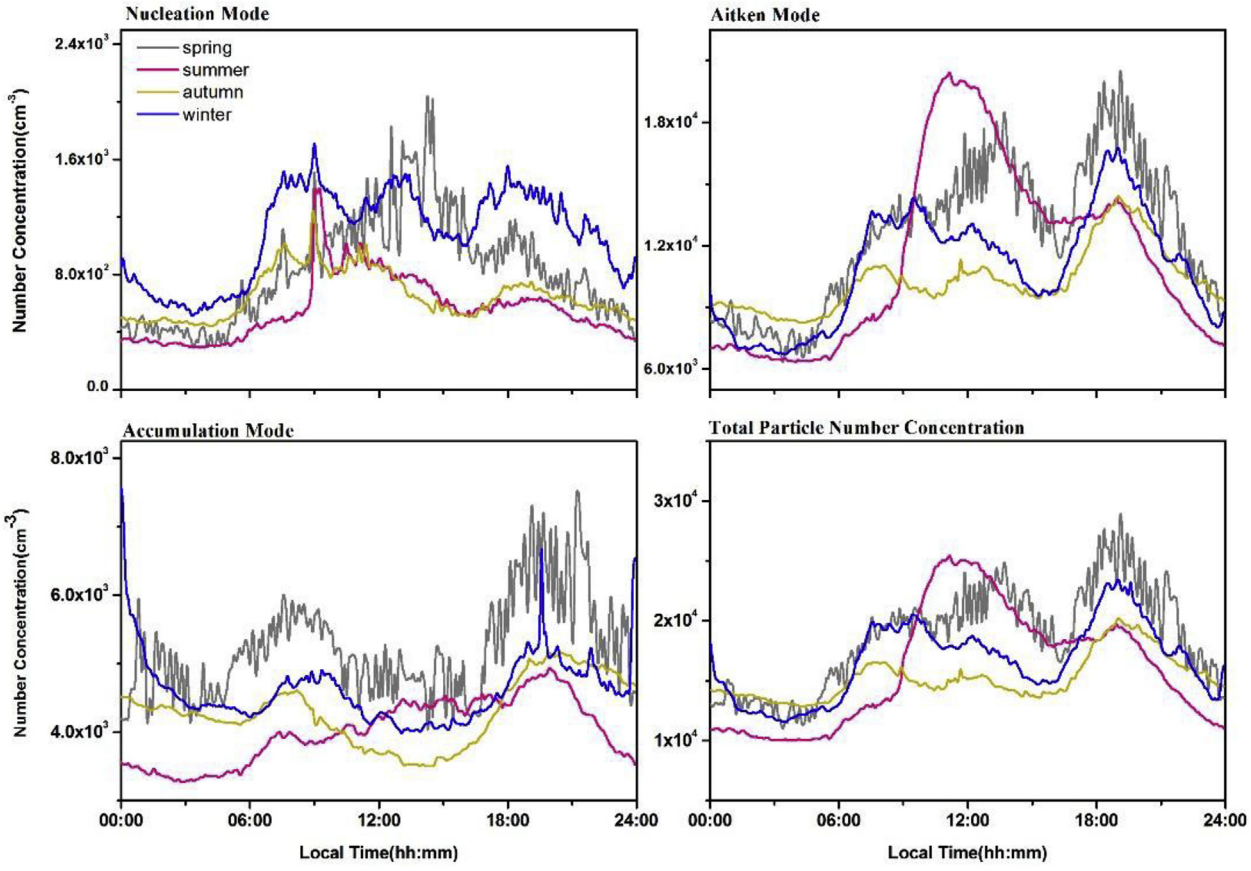

Fig. 3. Diurnal cycle of mean size-model and total particle number concentrations in four seasons.

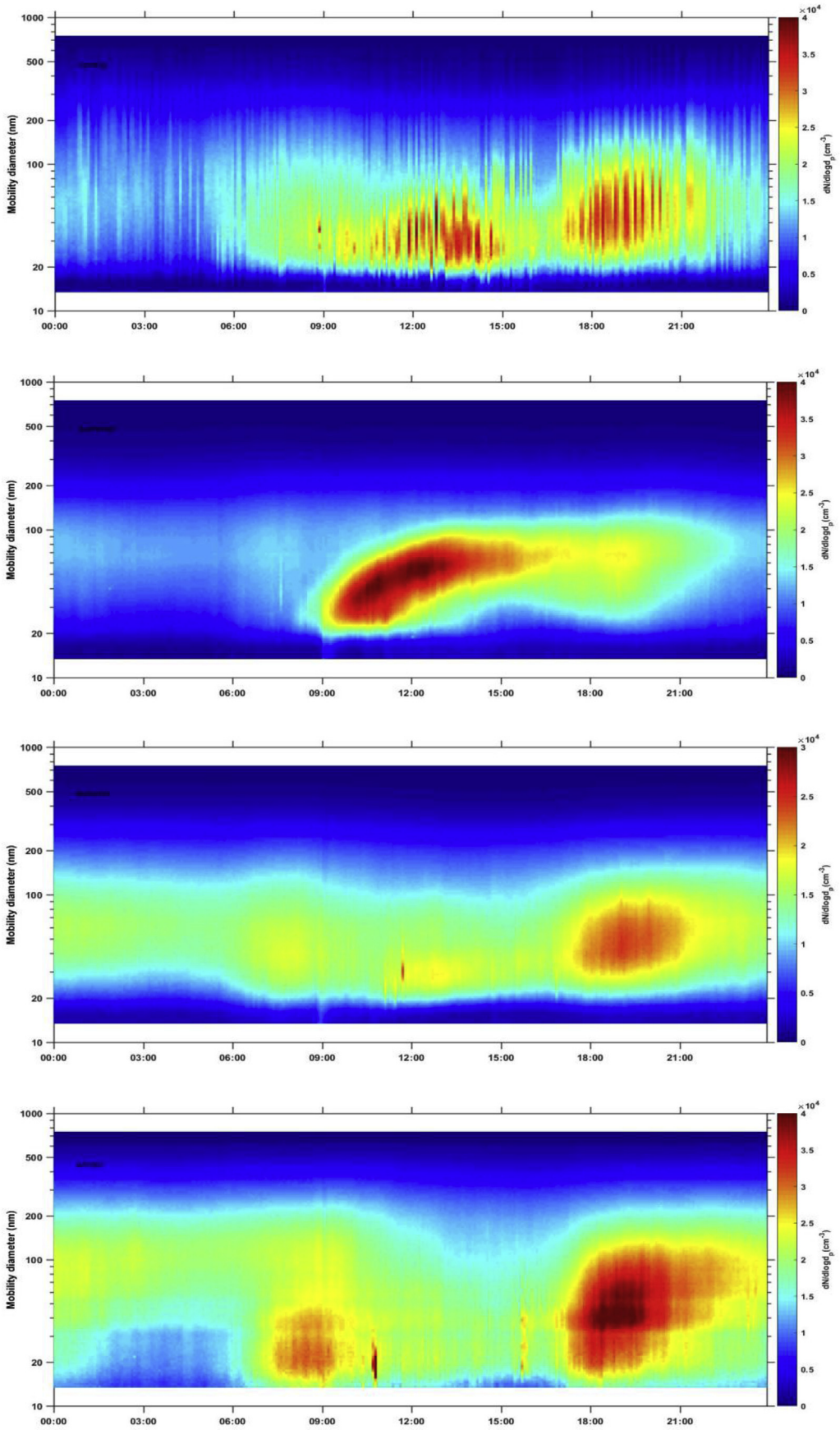

Fig. 4. Diurnal variation of particle number size distributions (13.5–600 nm) in four seasons.

Table 1
Key criterion for different pollution conditions.

Type	Visibility (km)	Relative humidity (%)	Episode
I	VIS ≥ 10	RH ≤ 80	Clean
II	5 ≤ VIS < 10	80 < RH ≤ 90	Mist
III	VIS < 5	80 < RH ≤ 90	Transition from mist to fog
IV	5 ≤ VIS < 10	RH ≤ 80	Haze
V	VIS < 5	RH ≤ 80	Heavy haze
VI	VIS < 10	RH > 90	Fog

(Vis) and relative humidity (RH) are important criteria for classifying weather conditions related to pollution, especially those containing particulate pollutants (Che et al., 2016). In this study, weather pollution conditions was categorized into six types according to an hourly time scale, that is, clean, haze, heavy haze, mist, a transition from mist to fog and fog, for the entire measurement period (Table 1). When Vis < 5 km and RH < 80%, the weather-pollution condition was defined as heavy haze. When Vis < 10 km and 80% < RH < 90%, the weather-pollution condition was categorized as a complex of co-occurring haze-fog or a transition episode (Leng et al., 2014, 2016).

During haze days, the hourly $PM_{2.5}$ often exceeded 90 μg m^{-3}, with the highest concentration of 602 μg m^{-3} on 6 December 2013. During the heavy haze days, the average hourly $PM_{2.5}$ reached 160.9 μg m^{-3} and 167.9 μg m^{-3} in spring and winter, respectively. Similar to particles that are generally more abundant in other periods, higher concentrations of gaseous precursors (e.g., SO_2, O_3, NO_2, NO, and NO_X) were also observed during normal and heavy haze periods. Additionally, low wind speeds were recorded during the whole study period compared to those on clean days (4.5 m s^{-1}), in particular, those during normal and heavy haze periods, with mean values of 3.5–3.8 m s^{-1}. The stagnant air caused by low wind speeds and weak convection was, to some extent, unfavorable for vertical diffusion or aerosol horizontal transport and therefore resulted in aerosol accumulation in the boundary layer.

Since the particle number size distribution data are on log scale, we transformed them into a linear scale by using a multiple-peak log-normal Gaussian fit ($y = y_0 + \frac{A}{\omega\sqrt{\pi/2}} e^{-\frac{(x-x_c)^2}{2\omega^2}}$), in which the particle median diameter is x_c, and the standard deviation is ω. We compared the mean particle number size distributions under different pollution conditions. The lowest number concentration of particles was found during fog rather than clean periods, which is partly because the relatively high RH could facilitate particle adsorption, dissolution and removal. For the transition period from mist to fog, the geometric mean diameter (GMD) was as high as that during the haze period, while the particle number concentration was as low as that during the clean period. Compared with haze case periods, heavy haze case periods appeared more frequently under the condition with lower visibility and higher concentrations of $PM_{2.5}$ and PM_{10}. During the mist periods, the low particle number concentration was mainly dependent on the higher relative humidity, similar to the fog period in spring, summer and winter. Table 2 shows the results of the multipeak fitting. The first spectrum mainly comprised particles with small sizes, while the second spectrum contained large sizes, including most of the Aitken mode particles. The GMD of the first spectrum was usually centered at 25–35 nm; however, the maximum (60.8 nm) occurred during the heavy hazy period in summer, and the minimum (15.1 nm) occurred during the mist period in spring. The second spectrum always had the highest GMD (75–110 nm) during the heavy haze periods, except in winter, and the lowest GMD (45–80 nm) occurred during clean or mist periods. Since the fine particles mainly originate from NPFs, while the large particles mainly originate from local primary emissions and particle growth, we believe that the aerosol distribution in Shanghai is mainly influenced by these factors. Furthermore, unfavorable meteorological conditions of high RH, low wind speed and less rainfall were more conducive to haze formation (Tian et al., 2015), and the particles were transported remotely from the north during warmer periods, even during regional haze pollution. Therefore, the highest concentration of particles occurred, as expected, in the transition period in winter.

Table 2
The multi-peaks fit of aerosol distributions under different pollution conditions.

Season	Type	Peak1(nm)	σ_1	Peak2(nm)	σ_2
Spring	Clean	30.0	1.06	71.4	1.11
	Mist	15.1	1.01	46.6	1.02
	transition	29.0	1.01	82.0	1.04
	Haze	31.5	1.04	94.8	1.06
	heavy haze	31.4	1.02	106.7	1.07
	Fog	28.4	1.05	72.7	1.03
	Clean	28.7	1.06	61.7	1.02
	Mist	23.4	1.04	60.2	1.03
Summer	transition	23.7	1.05	56.5	1.03
	Haze	26.3	1.02	76.3	1.02
	heavy haze	60.8	1.01	133.6	1.05
	Fog	23.1	1.05	54.5	1.03
	Clean	30.0	1.06	67.8	1.06
	Mist	30.6	1.05	78.0	1.04
Autumn	transition	29.9	1.02	100.2	1.02
	Haze	30.1	1.03	97.7	1.04
	heavy haze	33.5	1.02	113.6	1.02
	Fog	33.3	1.03	85.5	1.05
	Clean	28.0	1.07	67.5	1.11
	Mist	32.3	1.03	118.9	1.06
Winter	Transition	32.1	1.02	110.6	1.03
	Haze	28.1	1.04	81.0	1.06
	heavy haze	30.7	1.02	109.1	1.04
	Fog	37.4	1.05	103.5	1.24

3.3. New particle formation events

The measurement days over the 1-year study period were classified into different categories based on whether there is a nucleation burst occurred. Similar to the methods used by Dal Maso et al. (2005) and Kulmala et al. (2012), the NPF event days were defined as Class I and Class II. The Class I refers to the NPF days when the GR and FR can be calculated with confidence and Class II refers to that when it was impossible to accurately calculate. Undefined events refers to particles measured at smallest sizes of SMPS, and there is either no growth or there is growth followed by shrinking. For example, days with unclear growth or growing Aitken mode particles were classified as undefined.

The total occurrence frequency of Class I, Class II and undefined days as well as the percentages of the three types in each month are shown in Fig. 5. Overall, there were 89 NPF days during the whole measurement period, including Class I, Class II and undefined days, accounting for 26.5% of the total effective measurement days (335 days). There were 73 Class I and Class II days in total, which mostly occurred in summer and usually began a few hours before noon. This fraction of NPF days (27%) in Shanghai was slightly higher than that in Xi'an (19%) but lower than that in Hong Kong (34%), Beijing (40%), Taicang (44%) and Nanjing (51%) (Wu et al., 2008; Gao et al., 2009; Guo et al., 2012; Qi et al., 2015; Peng et al., 2017). In some previous studies, the NPFs could not be classified into three groups; therefore, in this study, the NPF fraction refers to the ratio of days, excluding non-NPF days, to the total measurement days.

The frequency histogram of the NPF days was similar to that in Xi'an from November 2013 to December 2014. In addition, the summer seems to have the highest frequency of NPF events and the Class I and Class II days accounted for the most proportion. And the proportion of Class I in February was particularly high was probably due to the small sample size caused by the less NPF events occurred at that time. The NPF events usually occurred during warm seasons due to strong

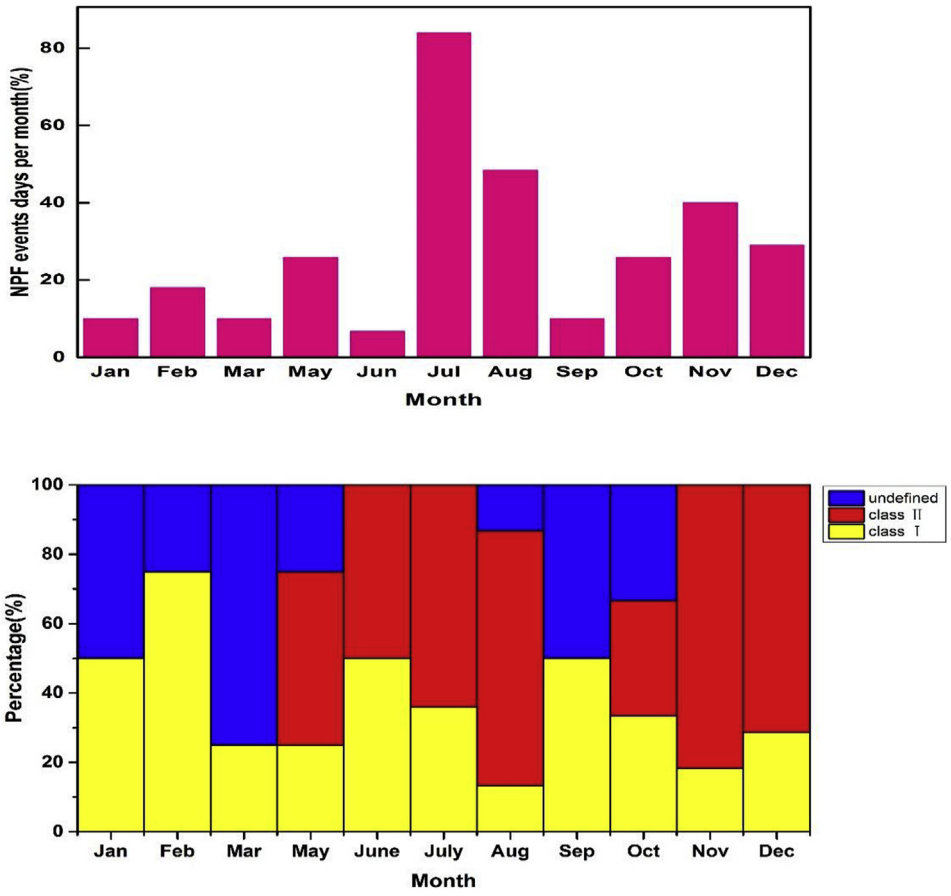

Fig. 5. Monthly frequency of new particle formation (NPF) event days.

biogenic activity, large emissions of biological volatile compounds and active solar radiation, especially in forested regions (Manninen et al., 2010). The solar radiation, as the driving force of NPF, provides more efficient photochemistry that promotes the formation of condensable vapors, such as sulfuric acid (Jaatinen et al., 2009; Pierce et al., 2014). Furthermore, other studies have demonstrated that NPFs favor conditions with stronger solar radiation, sufficient amounts of precursors, low-volatility organic condensable materials and low concentrations of preexisting aerosols (Pierce et al., 2014). Moreover, at our sample site in Shanghai, the NPF events occurred mainly at noon and continued for more than 2 h, sometimes up to 6–8 h. In addition, 40 NPF events were recorded in July and August, constituting 45% of the total NPF days. These events mainly happened in the morning (9:00–10:00 LT) and ended in the afternoon, continuing for more than 4 h.

3.3.1. Condensation sinks and coagulation sinks

Table 3 shows that the value of the calculated CS varies from 1.05×10^{-2} to 1.88×10^{-1} s^{-1} in NPF events during the four seasons, with a mean value and standard deviation of 5.31 (± 2.88)$\times10^{-2}$ s^{-1}. The highest CS occurred in winter, with a mean value and standard deviation of 8.26 (± 4.72) $\times10^{-2}$ s^{-1}. The mean CS value in Shanghai was considerably higher than that in other urban areas, for instance 1.43×10^{-2} s^{-1} in Paris (Dos Santos et al., 2015), 9.9×10^{-4} s^{-1} in Beijing (Wu et al., 2011) and 1.6×10^{-2} s^{-1} in Budapest (Salma et al., 2011). The CoagS values calculated during NPFs for particle sizes of 2 nm, 15 nm, 100 nm and 1000 nm are presented in Table 4. Here, the CoagS calculated from the CS using a diameter of 15 nm in formula (5) ranged from 2.6×10^{-4} to 6.3×10^{-4} s^{-1}, with the minimum value observed in summer and maximum in winter. It is obvious that the mean coagulation sink in summer was lower than that during the other seasons, which is in accordance with the high frequency of NPFs and the higher number concentration of nucleation particles.

Table 3
Condensation sink during NPF events in four seasons.

Condensation Sink (s^{-1})				
Season	Minimum	Maximum	Mean	Standard Deviation
spring	1.05×10^{-2}	7.37×10^{-2}	4.84×10^{-2}	2.53×10^{-2}
summer	1.54×10^{-2}	6.27×10^{-2}	3.37×10^{-2}	1.20×10^{-2}
autumn	1.11×10^{-2}	9.11×10^{-2}	4.75×10^{-2}	2.42×10^{-2}
winter	2.16×10^{-2}	1.88×10^{-1}	8.26×10^{-2}	4.72×10^{-2}

3.3.2. Growth rate and formation rate

The resultant GR was 0.1–15.5 nm h^{-1} with an average of 6.28 nm h^{-1}, which was within the range of the typical particle GR of 0.1–20 nm h^{-1} for global clean and polluted environments. Higher GR values have been observed in New Delhi (11.6–18.1 nm h^{-1}) and Mexico City (0.5–9 nm h^{-1}) (Dunn et al., 2004; Mönkkönen et al., 2005). Comparable GR values have been measured in Beijing (4 nm h^{-1}) as well as in Taicang (3.6–7.4 nm h^{-1}) and Shanghai (3.3–5.5 nm h^{-1}) (Gao et al., 2009; Yue et al., 2009; Du et al., 2012).

Table 4
Coagulation sink during NPF events in four seasons.

Season	Coag2 (s^{-1})	Coag15 (s^{-1})	Coag100 (s^{-1})	Coag1000 (s^{-1})
spring	9.2×10^{-3}	3.7×10^{-4}	1.8×10^{-5}	4.4×10^{-7}
summer	6.4×10^{-3}	2.6×10^{-4}	1.2×10^{-5}	3.1×10^{-7}
autumn	9.1×10^{-3}	3.6×10^{-4}	1.7×10^{-5}	4.4×10^{-7}
winter	1.57×10^{-2}	6.3×10^{-4}	3.0×10^{-5}	7.6×10^{-7}

Table 5
Growth rate and formation rate during NPF events.

Growth rate (GR) and Formation rate (J_{15})				
	Minimum	Maximum	Mean	Standard deviation
GR (nm hour^{-1})	0.10	15.50	6.28	5.16
J_{15} (cm^{-3} s^{-1})	0.02	2.54	0.37	0.50

Nevertheless, as for the formation rate, this calculation may greatly underestimate the particle production rate when the total particle number concentration is fairly high. Limited by the actual conditions of the measuring instruments, here, we only calculated the J_{15} of nucleation particles during NPFs (Table 5). The average J_{15} was 0.37 (± 0.5) cm^{-3} s^{-1}, which is far smaller than that in New Delhi (3.3–13.9 cm^{-3} s^{-1}), Atlanta (20-70 cm^{-3} s^{-1}) and Beijing (6 cm^{-3} s^{-1}) and is close to that reported in Taicang (1.2–2.5 cm^{-3} s^{-1}), a small city in the northwest of Shanghai (Kulmala et al., 2004a; Mönkkönen et al., 2005; Gao et al., 2009; Yue et al., 2009).

3.4. The potential role of VOCs in NPF events

Previous studies using field measurements and laboratory studies have shown that BVOCs and AVOCs are largely involved in the nucleation process and potentially contribute to NPF (Kulmala et al., 2004a; Hatch et al., 2011; Guo et al., 2012). In this study, we mainly focused on the role of VOCs among NPFs in urban environment. The top-10 main components of atmospheric VOCs in Shanghai are ethane, propane, toluene, acetylene, ethylene, n-butane, 1-butane, m, p-xylenes, benzene and ethylbenzene, and the average concentrations ranges from 0.74 ppbv to 3.33 ppbv. Fig. 6 displays the average concentrations of the main VOC species during three seasons since the data for autumn are missing. All major VOC species reached their maximum concentration in winter because the meteorological conditions inhibited the diffusion of pollutants. Direct measurements in a boreal forest environment have shown a clear positive correlation of the GR of the nucleation particles with monoterpene, which is a dominant group of BVOCs emitted from vegetation (Tatekawa et al., 2011). While the findings of Wang et al. (2015) suggest that the effect of monoterpenes on NPF is not clear in a polluted urban environment, the light intensity becomes a more important factor. Yao et al. (2018) conducted long-term measurements in Shanghai and found that NPF events were favored on days with high sulfuric acid concentration, stronger solar radiation, higher concentration of O_3, lower relative humidity, and less NO_X. These authors also discovered that the NPFs in Shanghai were generally induced by photochemical reactions. (Yao et al., 2018).

In this study, some continuous NPF events were recorded, and a typical example is an episode that took place from the 6th to the 13th of August with an average NPF events growth rate of 2.69 nm h^{-1}. Fig. 7 displays the aerosol size spectra, $PM_{2.5}$, gas pollutants and meteorological conditions during this period. The wind frequently changed direction, and the average wind speed was 4.2 m s^{-1}. RH rarely exceeded 80%. SO_2 and NO_X shared the similar diurnal variation pattern, with two peaks in the morning and evening commuting peak hours and one low value in between. There was a small time delay of approximately half an hour after reaching the morning rush hour before an increase in nucleation particles, which may be the time that the newly formed particles took to grow into a detectable size. Since sulfuric acid has been discovered would participates in the nucleation and growth of clusters, and SO_2 is needed for the production of sulfuric acid as well (Yao et al., 2018). In addition, anthropogenic and biogenic VOCs with nitrogen oxides (NO_X) are vital precursors of surface-level ozone, and the oxidation products of photochemical reactions play an important role to some extent in nucleation events (Guo et al., 2012). Surface-level ozone should be the precursor of NPF since it is involved in producing condensable species by reacting directly with VOCs and indirectly with generating oxidants, such as OH and HO_2, via photolysis (Jaatinen et al., 2009).

Mononuclear aromatics that originate mainly from similar sources, with the largest fractions derived from traffic emissions, are representative of VOC species emitted from anthropogenic activities in megacities (So and Wang, 2004). During this study, we observed enhanced concentrations of benzene and toluene, two typical anthropogenic aromatics, which coincided approximately with NPF events. Since the ratios of the two VOC species from common sources would not be affected by the mixing processes and photochemical reactions after they are emitted into the atmosphere, the mean ratio of toluene to benzene (T/B) represents the evaporation loss during refueling, storage and car exhausts. During this measurement period, the value of T/B was 2, which is typically characteristic of traffic emissions (Rappengluck et al., 1998). Additionally, a similar characteristic has also been

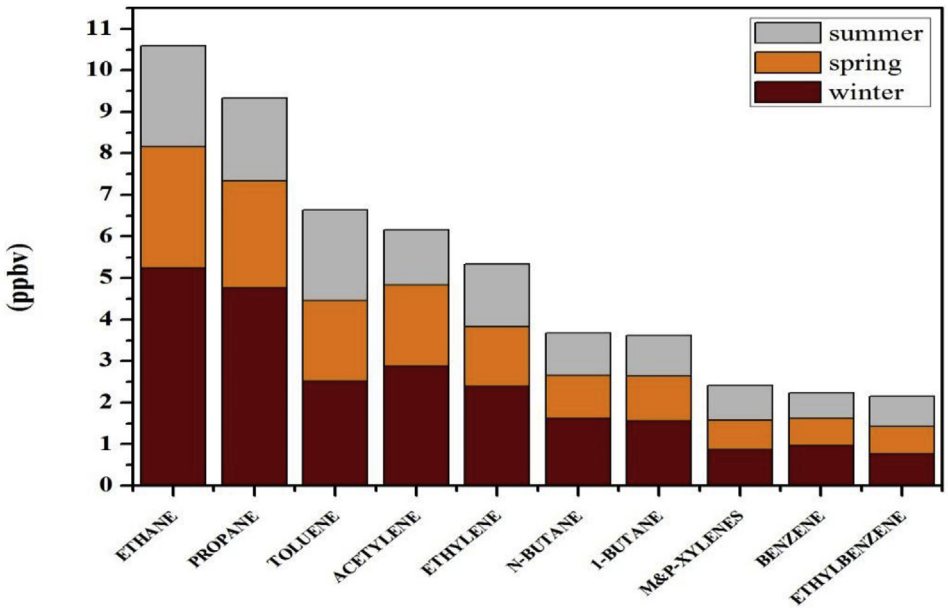

Fig. 6. Mean concentrations of top-10 typical VOCs species in spring, summer and winter.

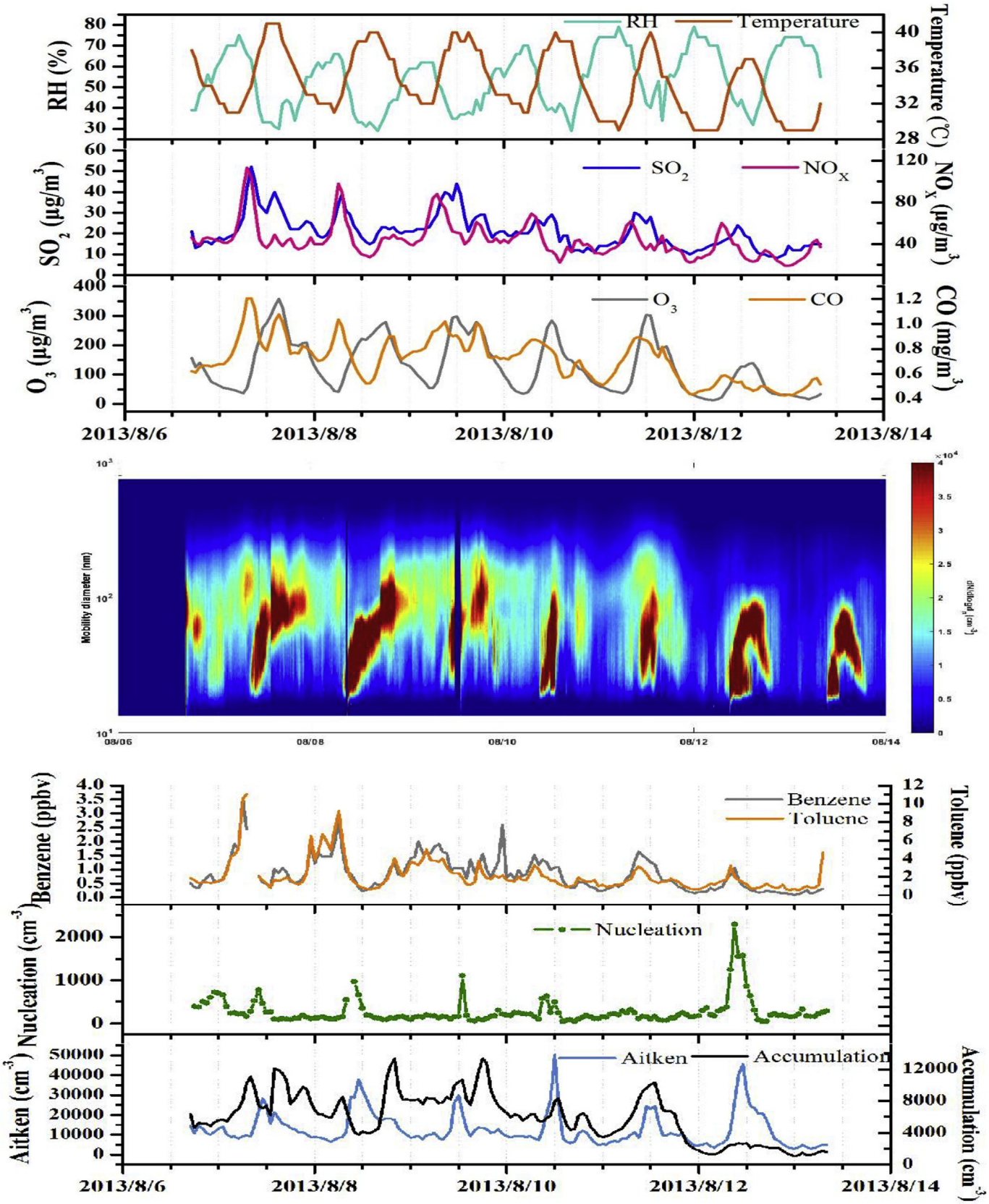

Fig. 7. Contour plots of particle number size distribution, meteorological conditions and concentrations of several gas pollutants and two VOCs species during 6–13 August in Shanghai.

Table 6
Linear correlations of gaseous pollutants, metrological parameters, CS, and AVOCs with the GR and CS for all NPF events observed during the sampling campaign. The data points for gaseous pollutants, metrological parameters and CS are 76 and 25 for AVOCs.

Parameter	Gaseous pollutants				Metrological parameters		CS	AVOC		
R	SO_2	O_3	NO_X	CO	T	RH	CS	Acetylene	Benzene	Toluene
GR	0.03	0.12	0.02	0.07	0.13	0.02	0.02	0.20	0.01	0.32
CS	0.64	−0.31	0.78	0.82	−0.48	−0.23	–	0.73	0.57	0.4

reported in laboratory studies, where anthropogenic aromatic photo-oxidation can drive nucleation and growth with or without H_2SO_4 (Metzger and Finlayson-Pitts, 2010). It is apparent that there is a relationship between aromatic hydrocarbons and the drivers of NPF events. Direct evidence of the participation of organic vapors in the nucleation process has already been discovered, where homomolecular nucleation of aromatic acids and sulfuric acid promoted efficient heteromolecular nucleation (Zhang et al., 2004b). Therefore, we suggest that mononuclear aromatics as organic vapors may, to some extent, contribute to the initial growth of the nucleation process. Furthermore, further research is needed to analyze the adsorption and heterogeneous reactions of organic vapors for subsequent particle growth.

We compared the GR to the concentrations of several VOCs during the study period (Fig. 7) and produced linear correlations of gaseous pollutants, metrological parameters, CS, and anthropogenic VOCs with the GR and CS for all observed NPF events (Table 6). Clearly, no notable correlations exist between GR and VOCs ($R < 0.3$). This noncorrelation situation may be caused by the uncertainty in the calculated GR. Other studies have encountered the same situation, where the correlation between GR and monoterpene was weak in most situations, and a positive correlation occurred only under specific temperature conditions and particle size ranges (Tatekawa et al., 2011). According to the binary and ternary nucleation models, some researches discovered that NPFs are highly dependent on H_2SO_4 and are dominated by other precursors such as NH_3 and VOC (Shen et al., 2016). Furthermore, Wang et al. (2015) recently discovered that the growth of nucleation particles was impacted by organic precursors based on a positive correlation between the growth rates and the organic vapors oxidized by ozone. Jiang et al. (2018) studied NPF in the photo-oxidation of aromatic hydrocarbons and discovered that, because of the neutrality of $PM_{2.5}$, the aggregation between VOC and VOC, VOC and sulfuric acid, VOC and ammonia and VOC and amines is caused by stable hydrogen bonding, while the aggregations among sulfuric acid, ammonia and amines are caused by the irreversible chemical reaction. In general, NPF events favor conditions with more intense solar radiation, sufficient amounts of precursor low-volatility organic condensable materials and low concentrations of preexisting aerosols (Pierce et al., 2014). In summary, the NPF events in Shanghai are, to a large degree, impacted by the mononuclear aromatics (e.g., Benzene, Toluene) from traffic emissions, but this influence is limited and results in weak correlations ($R = 0.2–0.32$) due to other changeable metrological factors. However, further evidence from smog chamber studies or molecular-level studies should be provided, and the exact contribution of VOCs to the formation and growth new particles is yet to be elucidated.

4. Summary and conclusions

A 1-year dataset of particle number size distributions measured in Shanghai in 2013 was used to explore the role of VOCs in NPF events in urban environments. The results show that Aitken particles play the leading role in the fluctuations of the total particle loadings, making up 60–70% of the total. The particle number size distributions have a similar pattern to diurnal variations in spring, autumn and winter, and an apparent 'banana' shape in summer. NPFs usually begin in the late morning and end in the afternoon. In total, 89 events were observed during the measurement period, accounting for 27% of the effective days. There is no clear correlation between the growth rate of NPFs and VOCs; however, an apparent good correlation was observed between nucleation particles and anthropogenic aromatic VOCs of benzene and toluene from traffic emissions.

This study sheds light on aerosol size distributions and NPF events. Although anthropogenic VOCs such as aromatics are known to contribute to the growth of newly formed particles, to better understand the role of VOCs in NPFs, more long-term measurements and additional modeling work should be conducted in the future.

Conflicts of interest

The authors declared that they have no conflicts of interest to this work. We declare that we do not have any commercial or associative interest that represents a conflict of interest in connection with the work submitted.

Acknowledgments

This research is supported by the National Key R&D Program of China (2016YFC0202003, 2017YFC1501405), the National Natural Science Foundation of China (41475026, 21507088, 41775129, 91637101, 41475109), and partly by the Science and Technology Innovation Project of Shanghai Academy of Environmental Sciences (CX201402) and the Science and Technology Commission of Shanghai Municipality (16ZR1431700). We would like to thank the anonymous reviewers, whose useful comments have improved the paper.

Appendix A. Supplementary data

Supplementary data to this article can be found online at https://doi.org/10.1016/j.atmosenv.2019.01.018.

References

Allan, J.D., Alfarra, M.R., Bower, K.N., Coe, H., Jayne, J.T., Worsnop, D.R., Aalto, P.P., Kulmala, M., Hyötyläinen, T., Cavalli, F., 2006. Size and composition measurements of background aerosol and new particle growth in a Finnish forest during QUEST 2 using an Aerodyne Aerosol Mass Spectrometer. Atmos. Chem. Phys. 6, 315–327.

Asmi, E., Frey, A., Virkkula, A., Ehn, M., Manninen, H., Timonen, H., Tolonen-Kivimäki, O., Aurela, M., Hillamo, R., Kulmala, M., 2010. Hygroscopicity and chemical composition of Antarctic sub-micrometre aerosol particles and observations of new particle formation. Atmos. Chem. Phys. 10, 4253–4271.

Che, H., Zhang, X., Wang, Y., Zhang, L., Shen, X., Zhang, Y., Ma, Q., Sun, J., Zhang, Y., Wang, T., 2016. Characterization and parameterization of aerosol cloud condensation nuclei activation under different pollution conditions. Sci. Rep. 6, 24497.

Creamean, J.M., Ault, A.P., Ten Hoeve, J.E., Jacobson, M.Z., Roberts, G.C., Prather, K.A., 2011. Measurements of aerosol chemistry during new particle formation events at a remote rural mountain site. Environ. Sci. Technol. 45, 8208–8216.

Dal Maso, M., Kulmala, M., Lehtinen, K.E., Mäkelä, J., Aalto, P., O'Dowd, C., 2002. Condensation and coagulation sinks and formation of nucleation mode particles in coastal and boreal forest boundary layers. J. Geophys. Res. 107.

Dal Maso, M., Kulmala, M., Riipinen, I., Wagner, R., Hussein, T., Aalto, P.P., Lehtinen, K.E., 2005. Formation and growth of fresh atmospheric aerosols: eight years of aerosol size distribution data from SMEAR II, Hyytiala, Finland. Boreal Environ. Res. 10, 323.

Dal Maso, M., Sogacheva, L., Aalto, P.P., Riipinen, I., Komppula, M., Tunved, P., Korhonen, L., SUUR-USKI, V., Hirsikko, A., Kurten, T., 2007. Aerosol size distribution measurements at four Nordic field stations: identification, analysis and trajectory analysis of new particle formation bursts. Tellus B 59, 350–361.

Dos Santos, V., Herrmann, E., Manninen, H., Hussein, T., Hakala, J., Nieminen, T., Aalto, P., Merkel, M., Wiedensohler, A., Kulmala, M., 2015. Variability of air ion

concentrations in urban Paris. Atmos. Chem. Phys. 15, 13717–13737.
Du, J., Cheng, T., Zhang, M., Chen, J., He, Q., Wang, X., Zhang, R., Tao, J., Huang, G., Li, X., 2012. Aerosol size spectra and particle formation events at urban Shanghai in Eastern China. Aerosol Air Qual. Res. 12, 1362–1372.
Dunn, M.J., Jiménez, J.L., Baumgardner, D., Castro, T., McMurry, P.H., Smith, J.N., 2004. Measurements of Mexico City nanoparticle size distributions: observations of new particle formation and growth. Geophys. Res. Lett. 31.
Gao, J., Wang, T., Zhou, X., Wu, W., Wang, W., 2009. Measurement of aerosol number size distributions in the Yangtze River delta in China: formation and growth of particles under polluted conditions. Atmos. Environ. 43, 829–836.
Guo, H., Wang, D., Cheung, K., Ling, Z., Chan, C.K., Yao, X., 2012. Observation of aerosol size distribution and new particle formation at a mountain site in subtropical Hong Kong. Atmos. Chem. Phys. 12, 9923–9939.
Han, Y., Iwamoto, Y., Nakayama, T., Kawamura, K., Hussein, T., Mochida, M., 2013. Observation of new particle formation over a mid-latitude forest facing the North Pacific. Atmos. Environ. 64, 77–84.
Harrison, R.M., Jones, M., Collins, G., 1999. Measurements of the physical properties of particles in the urban atmosphere. Atmos. Environ. 33, 309–321.
Hatch, L.E., Creamean, J.M., Ault, A.P., Surratt, J.D., Chan, M.N., Seinfeld, J.H., Edgerton, E.S., Su, Y., Prather, K.A., 2011. Measurements of isoprene-derived organosulfates in ambient aerosols by aerosol time-of-flight mass spectrometry-Part 1: single particle atmospheric observations in Atlanta. Environ. Sci. Technol. 45, 5105–5111.
Hussein, T., Puustinen, A., Aalto, P.P., Mäkelä, J.M., Hämeri, K., Kulmala, M., 2004. Urban aerosol number size distributions. Atmos. Chem. Phys. 4, 391–411.
Jaatinen, A., Hamed, A., Joutsensaari, J., Mikkonen, S., Birmili, W., Wehner, B., Spindler, G., Wiedensohler, A., Decesari, S., Mircea, M., 2009. A comparison of new particle formation events in the boundary layer at three different sites in Europe. Boreal Environ. Res. 14.
Jeong, K., 2009. Condensation of Water Vapor and Sulfuric Acid in Boiler Flue Gas. Dissertations & Theses. Gradworks.
Jiang, B., Xia, D., Zhang, X., 2018. A multicomponent kinetic model established for investigation on atmospheric new particle formation mechanism in H2SO4-HNO3-NH3-VOC system. Sci. Total Environ. 616, 1414–1422.
Khlystov, A., Stanier, C., Pandis, S.N., 2004. An algorithm for combining electrical mobility and aerodynamic size distributions data when measuring ambient aerosol special issue of aerosol science and technology on findings from the fine particulate matter supersites program. Aerosol Sci. Technol. 38, 229–238.
Kivekäs, N., Sun, J., Zhan, M., Kerminen, V.-M., Hyvärinen, A., Komppula, M., Viisanen, Y., Hong, N., Zhang, Y., Kulmala, M., 2009. Long term particle size distribution measurements at Mount Waliguan, a high-altitude site in inland China. Atmos. Chem. Phys. 9, 5461–5474.
Koponen, I.K., Virkkula, A., Hillamo, R., Kerminen, V.M., Kulmala, M., 2003. Number size distributions and concentrations of the continental summer aerosols in Queen Maud Land, Antarctica. J. Geophys. Res. 108.
Kulmala, M., Laakso, L., Lehtinen, K., Riipinen, I., Maso, M.D., Anttila, T., Kerminen, V.-M., Horrak, U., Vana, M., Tammet, H., 2004a. Initial steps of aerosol growth. Atmos. Chem. Phys. 4, 2553–2560.
Kulmala, M., Lehtinen, K.E.J., Laaksonen, A., 2006. Cluster activation theory as an explanation of the linear dependence between formation rate of 3nm particles and sulphuric acid concentration. Atmos. Chem. Phys. 6, 182–197.
Kulmala, M., Petäjä, T., Nieminen, T., Sipilä, M., Manninen, H.E., Lehtipalo, K., Dal Maso, M., Aalto, P.P., Junninen, H., Paasonen, P., 2012. Measurement of the nucleation of atmospheric aerosol particles. Nat. Protoc. 7, 1651.
Kulmala, M., Riipinen, I., Sipilä, M., Manninen, H.E., Petäjä, T., Junninen, H., et al., 2007. Toward direct measurement of atmospheric nucleation. Science 318 (5847), 89–92.
Kulmala, M., Vehkamäki, H., Petäjä, T., Dal Maso, M., Lauri, A., Kerminen, V.-M., Birmili, W., McMurry, P., 2004b. Formation and growth rates of ultrafine atmospheric particles: a review of observations. J. Aerosol Sci. 35, 143–176.
Lehtinen, K.E., Dal Maso, M., Kulmala, M., Kerminen, V.-M., 2007. Estimating nucleation rates from apparent particle formation rates and vice versa: revised formulation of the Kerminen–Kulmala equation. J. Aerosol Sci. 38, 988–994.
Leng, C., Duan, J., Xu, C., Zhang, H., Wang, Y., Wang, Y., Li, X., Kong, L., Tao, J., Zhang, R., 2016. Insights into a historic severe haze event in Shanghai: synoptic situation, boundary layer and pollutants. Atmos. Chem. Phys. 16, 9221–9234.
Leng, C., Zhang, Q., Tao, J., Zhang, H., Zhang, D., Xu, C., Li, X., Kong, L., Cheng, T., Zhang, R., 2014. Impacts of new particle formation on aerosol cloud condensation nuclei (CCN) activity in Shanghai: case study. Atmos. Chem. Phys. 14, 11353–11365.
Li, L., Chen, C., Fu, J., Huang, C., Streets, D., Huang, H., et al., 2011. Air quality and emissions in the Yangtze River Delta, China. Atmos. Chem. Phys. 11, 1621–1639.
Mönkkönen, P., Koponen, I., Lehtinen, K., Hämeri, K., Uma, R., Kulmala, M., 2005. Measurements in a highly polluted Asian mega city: observations of aerosol number size distribution, modal parameters and nucleation events. Atmos. Chem. Phys. 5, 57–66.
Manninen, H., Nieminen, T., Asmi, E., Gagné, S., Häkkinen, S., Lehtipalo, K., Aalto, P., Vana, M., Mirme, A., Mirme, S., 2010. EUCAARI ion spectrometer measurements at 12 European sites–analysis of new particle formation events. Atmos. Chem. Phys. 10, 7907–7927.
Massman, W., 1998. A review of the molecular diffusivities of H2O, CO2, CH4, CO, O3, SO2, NH3, N2O, NO, and NO2 in air, O2 and N2 near STP. Atmos. Environ. 32, 1111–1127.
Metzger, A., Finlayson-Pitts, B.J., 2010. Evidence for the role of organics in aerosol particle formation under atmospheric conditions. Proc. Natl. Acad. Sci. U.S.A. 107, 6646–6651.
Pérez, N., Pey, J., Cusack, M., Reche, C., Querol, X., Alastuey, A., Viana, M., 2010. Variability of particle number, black carbon, and PM, PM, and PMLevels and speciation: influence of road traffic emissions on urban air quality. Aerosol Sci. Technol. 44, 487–499.
Peng, Y., Liu, X., Dai, J., Wang, Z., Dong, Z., Dong, Y., Chen, C., Li, X., Zhao, N., Fan, C., 2017. Aerosol size distribution and new particle formation events in the suburb of Xi'an, northwest China. Atmos. Environ. 153, 194–205.
Penner, J.E., Dong, X.Q., Chen, Y., 2004. Observational evidence of a change in radiative forcing due to the indirect aerosol effect. Nature 427, 231–234.
Penttinen, P., Timonen, K.L., Tiittanen, P., Mirme, A., Ruuskanen, J., Pekkanen, J., 2001. Number concentration and size of particles in urban air: effects on spirometric lung function in adult asthmatic subjects. Environ. Health Perspect. 109, 319.
Pierce, J., Adams, P., 2009. Uncertainty in global CCN concentrations from uncertain aerosol nucleation and primary emission rates. Atmos. Chem. Phys. 9, 1339–1356.
Pierce, J., Leaitch, W., Liggio, J., Westervelt, D., Wainwright, C., Abbatt, J., Ahlm, L., Al-Basheer, W., Cziczo, D., Hayden, K., 2012. Nucleation and condensational growth to CCN sizes during a sustained pristine biogenic SOA event in a forested mountain valley. Atmos. Chem. Phys. 12, 3147–3163.
Pierce, J., Westervelt, D., Atwood, S., Barnes, E., Leaitch, W., 2014. New-particle formation, growth and climate-relevant particle production in Egbert, Canada: analysis from 1 year of size-distribution observations. Atmos. Chem. Phys. 14, 8647–8663.
Pikridas, M., Riipinen, I., Hildebrandt, L., Kostenidou, E., Manninen, H., Mihalopoulos, N., Kalivitis, N., Burkhart, J.F., Stohl, A., Kulmala, M., 2012. New particle formation at a remote site in the eastern Mediterranean. J. Geophys. Res. 117.
Qi, X.M., Ding, A.J., Nie, W., Petäjä, T., Kerminen, V.M., Herrmann, E., Xie, Y., Zheng, L., Manninen, H., Aalto, P., 2015. Aerosol size distribution and new particle formation in the western Yangtze River Delta of China: two-year measurement at the sorpes station. Atmos. Chem. Phys. 15 (8), 12445–12464.
Rappengluck, B., Fabian, P., Kalabokas, P., Viras, L.G., Ziomas, I.C., 1998. Quasi-continuous measurements of non-methane hydrocarbons (NMHC) in the greater Athens area during MEDCAPHOT-TRACE. Atmos. Environ. 32, 2103–2121.
Salma, I., Borsós, T., Weidinger, T., Aalto, P., Hussein, T., Dal Maso, M., Kulmala, M., 2011. Production, growth and properties of ultrafine atmospheric aerosol particles in an urban environment. Atmos. Chem. Phys. 11, 1339.
Sarnat, J.A., Schwartz, J., Suh, H.H., 2001. Fine particulate air pollution and mortality in 20 U.S. cities. N. Engl. J. Med. 344, 1253–1254.
Seinfeld, J.H., Pandis, S.N., 2006. Atmospheric Chemistry and Physics: from Air Pollution to Climate Change, second ed. John Wiley & Sons, New York.
Shen, X.J., Sun, J.Y., Zhang, X.Y., Zhang, Y.M., Zhang, L., Fan, R.X., Zhang, Z.X., Zhang, X.L., Zhou, H.G., Zhou, L.Y., 2016. The influence of emission control on particle number size distribution and new particle formation during China's V-Day parade in 2015. Sci. Total Environ. 573, 409–419.
Siingh, D., Gautam, A., Kamra, A., Komsaare, K., 2013. Nucleation events for the formation of charged aerosol particles at a tropical station—preliminary results. Atmos. Res. 132, 239–252.
So, K., Wang, T., 2004. C3–C12 non-methane hydrocarbons in subtropical Hong Kong: spatial–temporal variations, source–receptor relationships and photochemical reactivity. Sci. Total Environ. 328, 161–174.
Spracklen, D., Carslaw, K., Kulmala, M., Kerminen, V.-M., Mann, G., Sihto, S.-L., 2006. The contribution of boundary layer nucleation events to total particle concentrations on regional and global scales. Atmos. Chem. Phys. Discuss. 6, 7323–7368.
Stanier, C.O., Khlystov, A.Y., Pandis, S.N., 2004a. Ambient aerosol size distributions and number concentrations measured during the Pittsburgh Air Quality Study (PAQS). Atmos. Environ. 38, 3275–3284.
Stanier, C.O., Khlystov, A.Y., Pandis, S.N., 2004b. Nucleation events during the Pittsburgh Air Quality Study: description and relation to key meteorological, gas phase, and aerosol parameters special issue of aerosol science and technology on findings from the fine particulate matter supersites program. Aerosol Sci. Technol. 38, 253–264.
Tatekawa, Y., Kanehiro, H., Nakajima, Y., 2011. Growth rates of nucleation mode particles in Hyytiala during 2003-2009: variation with particle size, season, data analysis method and ambient conditions. Atmos. Chem. Phys. Discuss. 11, 12865–12886.
Tian, M., Wang, H.B., Chen, Y., Yang, F.M., Zhang, X.H., Zou, Q., Zhang, R.Q., Ma, Y.L., He, K.B., 2015. Characteristics of aerosol pollution during heavy haze events in Suzhou, China. Atmos. Chem. Phys. 16, 7357–7371.
Vakkari, V., Laakso, H., Kulmala, M., Laaksonen, A., Mabaso, D., Molefe, M., Kgabi, N., Laakso, L., 2011. New particle formation events in semi-clean South African savannah. Atmos. Chem. Phys. 11, 3333–3346.
Wang, H., Zhu, B., Shen, L., An, J., Yin, Y., Kang, H., 2014. Number size distribution of aerosols at Mt. Huang and Nanjing in the Yangtze River Delta, China: effects of air masses and characteristics of new particle formation. Atmos. Res. 150, 42–56.
Wang, Z., Hu, M., Pei, X., Zhang, R., Paasonen, P., Zheng, J., Yue, D., Wu, Z., Boy, M., Wiedensohler, A., 2015. Connection of organics to atmospheric new particle formation and growth at an urban site of Beijing. Atmos. Environ. 103, 7–17.
Weber, R., McMurry, P.H., Mauldin, R., Tanner, D., Eisele, F., Clarke, A., Kapustin, V., 1999. New particle formation in the remote troposphere: a comparison of observations at various sites. Geophys. Res. Lett. 26, 307–310.
Woo, K., Chen, D., Pui, D., McMurry, P., 2001. Measurement of Atlanta aerosol size distributions: observations of ultrafine particle events. Aerosol Sci. Technol. 34, 75–87.
Wu, Z., Hu, M., Lin, P., Liu, S., Wehner, B., Wiedensohler, A., 2008. Particle number size distribution in the urban atmosphere of Beijing, China. Atmos. Environ. Times 42, 7967–7980.
Wu, Z., Hu, M., Liu, S., Wehner, B., Bauer, S., Wiedensohler, A., Petäjä, T., Dal Maso, M., Kulmala, M., 2007. New particle formation in Beijing, China: statistical analysis of a 1-year data set. J. Geophys. Res. 112.
Wu, Z., Hu, M., Yue, D., Wehner, B., Wiedensohler, A., 2011. Evolution of particle number size distribution in an urban atmosphere during episodes of heavy pollution and new particle formation. Sci. China Earth Sci. 54, 1772.
Xiao, S., Wang, M., Yao, L., Kulmala, M., Zhou, B., Yang, X., Chen, J., Wang, D., Fu, Q.,

Worsnop, D., 2015. Strong atmospheric new particle formation in winter in urban Shanghai, China. Atmos. Chem. Phys. 15, 1769–1781.
Yao, L., Garmash, O., Bianchi, F., Zheng, J., Yan, C., Kontkanen, J., Junninen, H., Mazon, S.B., Ehn, M., Paasonen, P., 2018. Atmospheric new particle formation from sulfuric acid and amines in a Chinese megacity. Science 361, 278–281.
Yin, Z., Ye, X., Jiang, S., Tao, Y., Shi, Y., Yang, X., Chen, J., 2015. Size-resolved effective density of urban aerosols in Shanghai. Atmos. Environ. 100, 133–140.
Yue, D., Hu, M., Wang, Z., Wen, M., Guo, S., Zhong, L., Wiedensohler, A., Zhang, Y., 2013. Comparison of particle number size distributions and new particle formation between the urban and rural sites in the PRD region, China. Atmos. Environ. 76, 181–188.
Yue, D., Hu, M., Wu, Z., Wang, Z., Guo, S., Wehner, B., Nowak, A., Achtert, P., Wiedensohler, A., Jung, J., 2009. Characteristics of aerosol size distributions and new particle formation in the summer in Beijing. J. Geophys. Res. 114.
Zhang, Q., Ning, Z., Shen, Z., Li, G., Zhang, J., Lei, Y., Xu, H., Sun, J., Zhang, L., Westerdahl, D., 2017. Variations of aerosol size distribution, chemical composition and optical properties from roadside to ambient environment: a case study in Hong Kong, China. Atmos. Environ. 166, 234–243.
Zhang, Q., Streets, D.G., Carmichael, G.R., He, K., Huo, H., Kannari, A., et al., 2009. Asian emissions in 2006 for the NASA INTEX-B mission. Atmos. Chem. Phys. 9, 5131–5153.
Zhang, R., Suh, I., Zhao, J., Zhang, D., Fortner, E.C., Tie, X., Molina, L.T., Molina, M.J., 2004b. Atmospheric new particle formation enhanced by organic acids. Science 304, 1487–1490.

Further reading

Zhang, Q., Stanier, C.O., Canagaratna, M.R., Jayne, J.T., Worsnop, D.R., Pandis, S.N., Jimenez, J.L., 2004a. Insights into the chemistry of new particle formation and growth events in Pittsburgh based on aerosol mass spectrometry. Environ. Sci. Technol. 38, 4797–4809.